Journal of GeoEngineering, Vol. 14, No. 1, pp. 1-10, March 2019
http://dx.doi.org/10.6310/jog.201903_14(1).1

BEARING CAPACITY OF FREE-ROTATING AND RESTRAINED FOOTINGS NEAR SLOPES

Ching-Chuan Huang [1*] and Yue-Wen Chen [2]

ABSTRACT

Loading tests on model horizontal grounds and slopes are performed using a 100-mm-wide strip footing with restrained and free-rotation conditions. Test results reveal that complete restraint against rotations on the footing generates larger values of ultimate bearing capacity and deeper failure surfaces than those for footings with a free-rotation condition. This is true for horizontal and slanted grounds with various slope angles. Test results also reveal that for a vertically loaded footing, a major factor that influences the ultimate bearing capacity of the footing (q_u) is the load eccentricity (e_c) at the footing base. The influence of load inclination on the values of q_u for free-rotating and fixed footings is minor because the load inclination angles measured during the loading tests were negligibly small. In the case of a footing placed on a slanted ground, a load eccentric toward the heel of the footing is associated with a larger value of q_u than that for a load eccentric toward the toe of the footing when subjected to similar extents of load eccentricity. This observation suggests that the currently used formula for correcting load eccentricity (e_c) has to be updated in order to address the issue of increased q_u induced by a load eccentricity toward the heel of the footing.

Key words: Bearing capacity, model test, load inclination, load eccentricity.

1. INTRODUCTION

The ultimate bearing capacity of footings has been studied since the 1920's via theoretical analyses (Terzaghi 1943), large-scale loading tests (Briaud and Gibben 1999), reduce-scale model tests (Huang *et al.* 1994; Kumar and Chakraborty 2015), limit analyses (Ukritchon *et al.* 2003; Zhu and Michalowski 2005; Georgiadis 2010) and numerical analyses (Kotake *et al.* 2001; Sadoglu 2015). Formulas for evaluating the ultimate bearing capacity of a footing (q_u) and the correction factors for taking into account various boundary and loading conditions are well established (Meyerhof 1957, 1963; Hansen 1970; Vesic 1973, 1975). Foundation structures such as spread footings and piers receive various degrees of restraint from superstructures. In the case of placing a footing on (or adjacent to) a sloped ground, the footing may behave differently from that expected for the case of a footing placed on a horizontal ground (Meyerhof 1957; Huag and Kang 2008; Leshchinsky 2015; Leshchinsky and Xie 2017). In this case, the boundary condition is asymmetric to the center line of footing and the bearing capacity characteristics are sensitive the orientations of loading conditions such as inclined and eccentric loading. It was shown by Tatsuoka and Huang (1991) that the ultimate bearing capacity of footings can be strongly influenced by restraining the lateral movement and/or the rotation of the footing. The value of q_u for a surface strip footing situated on a horizontal or slanted ground consisting of a homogeneous cohesionless soil can be expressed using the following equation:

$$q_u = \frac{1}{2} \cdot B \cdot \gamma \cdot N_r \cdot g_\gamma \cdot i_\gamma \cdot e_\gamma \tag{1}$$

where
B: width of footing
γ: unit weight of soil
N_γ: bearing capacity factor for the effect of soil self-weight
g_γ: correction factor for ground inclination
i_γ: correction factor for load inclination
e_γ: correction factor for load eccentricity

Extensive studies have been conducted in order to obtain accurate values of N_γ, g_γ, i_γ, and e_γ (Meyerhof 1957, 1963; Hansen 1970; Vesic 1973, 1975; Purkayastha and Char 1977; Fishman and Yao 2003; Krabenhoft *et al.* 2013; Tang *et al.* 2017). However, the majority of these studies considered the case of a strip footing placed on a horizontal ground (El-Sawwaf 2009; El Sawwaf and Nazir 2012; Ganesh *et al.* 2017), for which a load eccentric toward either side of the footing yields identical values of q_u; *i.e.,* the values of e_γ are not influenced by the direction of eccentricity imposed on the strip footing because both the ground surface and the failure mechanism are symmetrical with respect to the centerline of the footing. However, this is not the case for a strip footing placed on (or near) the slope because in this case both the ground surface and the failure mechanism are asymmetrical with respect to the centerline of the footing. Studies on the characteristics of e_γ for an eccentrically loaded strip footing situated on a sloped ground are very limited (Cure *et al.* 2014). The present study thus conducted a series of model loading tests for a rigid strip footing placed on model grounds with various slope angles and restraining conditions.

2. MODEL TEST SETUP

Figure 1 shows the geometry of the model slope with various slope angles (β), ranging between 0° (horizontal ground) and

Manuscript received October 30, 2017; revised May 25, 2018; accepted August 17, 2018.
[1*] Professor (corresponding author), Department of Civil Engineering, National Cheng Kung University, Taiwan 70101, R.O.C. (e-mail: samhcc@mail.ncku.edu.tw).
[2] Formerly graduate student, Department of Civil Engineering, National Cheng Kung University, Taiwan 70101, R.O.C.

30°. Four types of model slope with various values of (β), namely β = 0° (level ground), 10°, 20°, and 30°, were built and loaded to failure states using a strip footing. A steel frame (2.5 m long, 1.0 m high, and 0.15 m wide) was established to contain a 500-mm-high model slope. The toe of 100 mm-wide strip footing is aligned with the line of flat-to-slope transition as shown in Fig. 2. A total of 5 load cells with dimensions of 20 mm (width) × 50 mm (height) × 150 mm (length) were rigidly attached to the base of the 100-mm-wide footing to measure the distributions of normal and shear stresses at the footing base. This enables a real-time evaluation of the load inclination and load eccentricity during the loading test. These load cells are capable of measuring normal and shear forces simultaneously with a negligibly small coupling effect, as reported in detail by Huang and Chen (2012a). Two displacement transducers were installed at the two sides of the footing to detect the vertical settlement as well as the rotation of the footing, as shown in Fig. 2. Figures 3(a) and 3(b) show close-up view on the free-rotating and fixed rigid strip footings, respectively. Two hinges were installed at a height of 50 mm above the center of the footing base to transfer the footing load from a screw jack (vertical displacement rate: 1 mm/min). The hinges were placed 50 mm above the center of the footing base to minimize possible load eccentricity during loading, as reported by Huang *et al.* (1994). Note that to investigate the influence of load inclination (or eccentricity) on the bearing capacity of footings, a constant load inclination angle (or a constant load eccentricity) throughout the loading test is required (*e.g.,* Tatsuoka *et al.* 1991; Huang *et al.* 1994). However, the present study aims at exploring failure mechanisms and responses of vertically loaded footings under different constraint conditions. As a result, both load inclination and load eccentricity variate during loading.

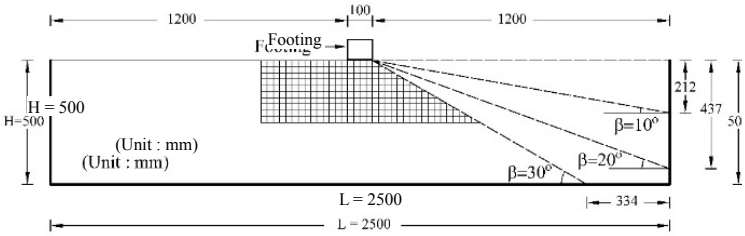

Fig. 1 Schematic views on the footing constraint conditions used in the tests

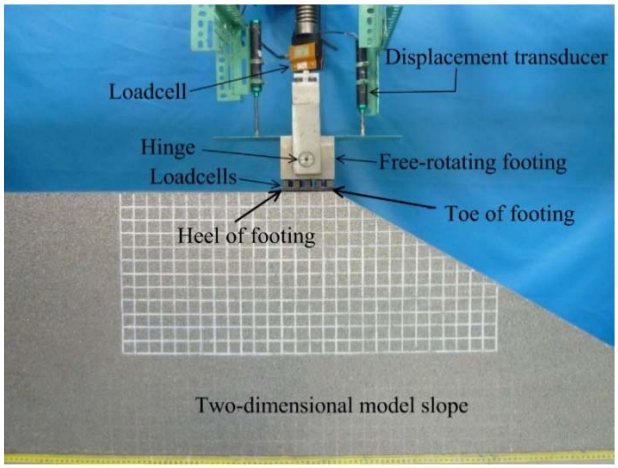

Fig. 2 Model test set-up

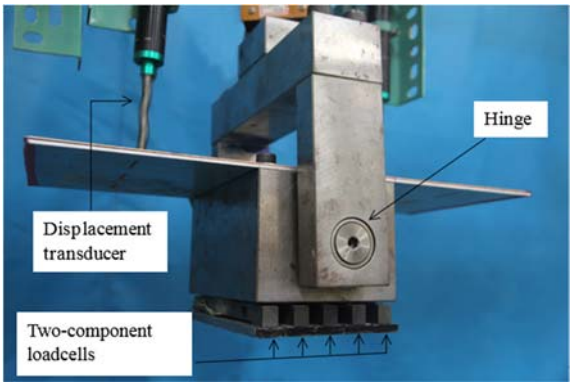

(a) Free-rotating footing

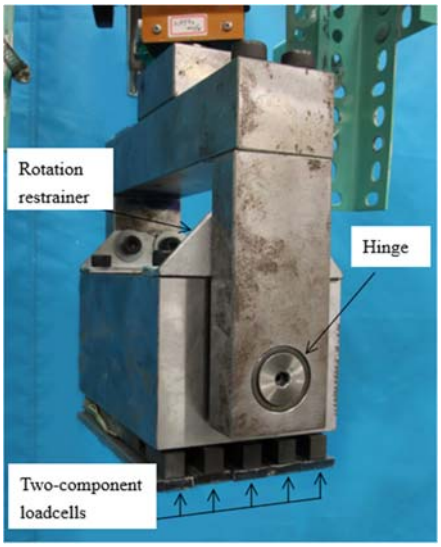

(b) Fixed footing

Fig. 3 Close view of footings

To achieve a rigidly jointed footing condition, two L-shaped steel plates were placed on the top of the footing to prevent it from rotating, as shown in Fig. 3(b). Figure 4(a) shows a schematic view of the medium-scale direct shear test apparatus, which consists of a 300-mm-wide, 150-mm-long, and 300-mm-high shear box (150 mm for the upper and lower halves, respectively, with a gap of 1 mm between them), a diaphragm cylinder regulated by an air pressure valve for applying normal pressures, and a crew jack for applying shear displacement to the lower half of the shear box. The upper half of the shear box is rigidly jointed to the frame of the testing system and the movement of lower half shear box is guided by two linear bearings. Figure 4(b) shows a close-up view on the shear boxes and specimen at a large shear displacement of 50 mm.

3. TEST MEDIUM

Stainless steel rods with a uniform diameter of 1.96 mm and a length of 150 mm were stacked in a rhombic pattern to simulate an idealized two-dimensional assembly of uniform cohesionless particles. The assembly of the stacked steel rods has a void ratio of 0.103 and a unit weight of γ = 68.5 kN/m^3, which is about 4 times that of a typical soil (γ = 17 kN/m^3). Therefore, the model consisting of steel rods simulates a 4*g* (*g*: gravitational acceleration) condition. This is equivalent to the stress level in a

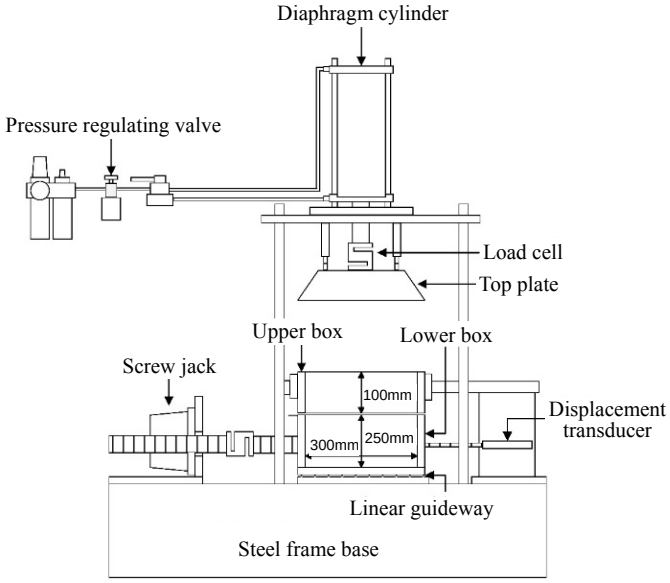

(a) Test set-up

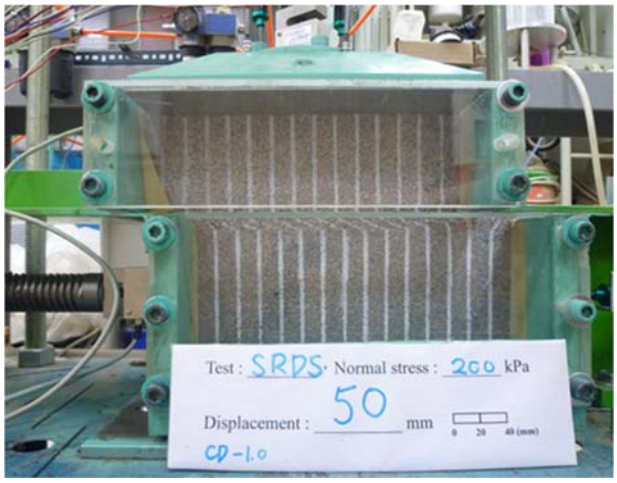

(b) Close view of the shear box and specimen at a large shear

Fig. 4 Direct shear apparatus for the idealized two-dimensional test medium

2.0-m-high (= 4 × 0.5 m) soil structure, avoiding the state of low stress level, as in the model. On the other hand, the use of a 1.96-mm-diameter steel rod simulates a diameter of 7.8 mm (= 4 × 1.96 mm), which can be classified as gravels according to the Unified Soil Classification System (ASTM D-2487) for a 2.0-m-high soil slope. Another feature of the tested material is that the Mohr-Coulomb failure envelope, which is commonly used for various soils, is also valid for the steel rods used here. This is discussed in detail later. Repeatability of the model slope configuration and the backfill density are a major advantage of using the steel rod assembly. This is because the steel rod assembly is formed by placing the steel rods piece-by-piece throughout the model slope construction. Therefore, the uncertainty associated with the construction of a model of steel rods is considered less than that of any other method of density control for soil specimens.

Figure 5(a) shows shear stress *vs.* shear displacement curves for various normal pressures (σ_n) in the range of 25 and 200 kPa obtained from direct shear tests on the steel rod assembly. It can be seen that the shear stress responded to the applied shear displacements in a periodic manner; *i.e.,* a shear displacement increase of about 2 mm (approximately the diameter of the steel rods) causes the upper layer of steel rods to climb over the lower layer of steel rods. This cyclic stress-displacement pattern is considered to be a unique feature of the constant-displacement-rate testing condition for the steel rod assembly. Simplified versions of Fig. 5(a) are shown in Fig. 5(b); they were obtained by eliminating the post-peak cyclic curves and connecting all points of peak stress to mimic a loading-rate-controlled test condition, as shown in Fig. 5(b), representing non-linearly elastic-plastic stress-displacement behavior. For the regular steel rod packing used here, the peak-residual cycles shown in Fig. 5(a) is a stress-displacement pattern existing only in the case of displacement-controlled tests. Theoretically, the shear stress at the "valley" of these cycles should be zero. However, this is not the case for the curves of 25 and 50 kPa due to minor friction forces existing at linear guideways at the bottom of the shear box. It is also noted that these "valleys" exist exclusively in displacement-rate-controlled shear tests. In reality, a ground subjected to loading-rate-controlled loading may be with more practical significance than that subjected to displacement-rate-controlled loading. In the case of loading-rate-controlled condition, these valleys disappear, and the material exhibits a "perfectly-plastic" property in post-peak regime, as shown in Fig. 5(b).

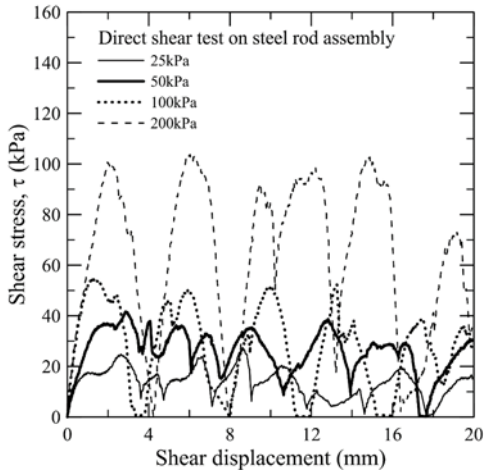

(a) Periodic shear-displacement behavior

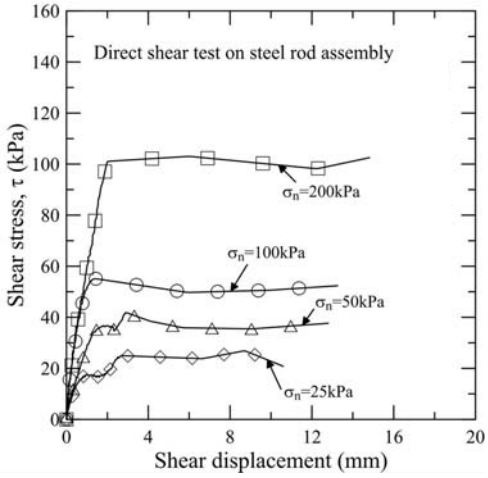

(b) Simplified small displacement behavior

Fig. 5 Stress-displacement curves obtained from the direct shear tests

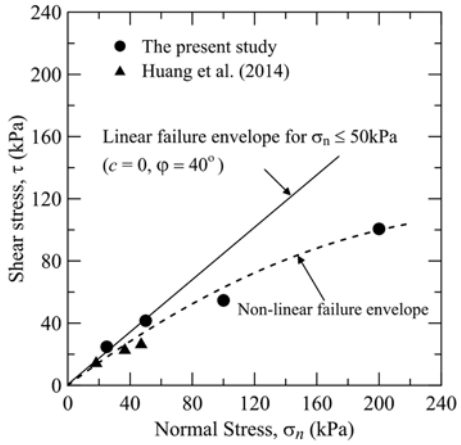

(a) Mohr-Coulomb failure envelope

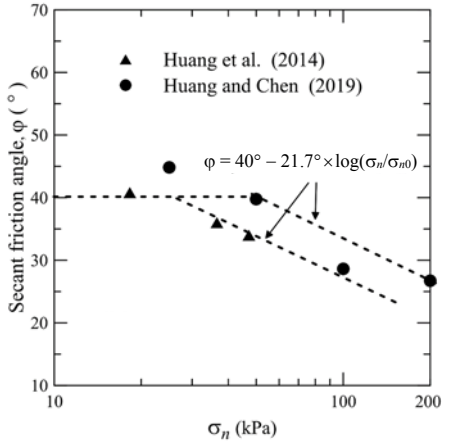

(b) φ-σ_n relationship

Fig. 6 Results of direct shear tests

Figures 6(a) and 6(b) show the curved Mohr-Coulomb failure envelope and the secant friction angles, respectively, for the test medium. The secant friction angle can be expressed using the following logarithmic function, which is widely used to take into account the influence of pressure levels on the secant friction angle (φ) of cohesionless soils (*e.g.,* Duncan and Wright 2005):

$$\varphi = 40° - 21.7° \times \log\left(\frac{\sigma_n}{\sigma_{n0}}\right) \quad (2)$$

where σ_{n0} is the reference normal pressure (= 30 ~ 50 kPa in the present study).

4. LOAD-SETTLEMENT RESPONSE OF FOOTINGS

Figure 7 shows two typical examples of average footing pressure (q) *vs.* normalized vertical footing displacement (S_v/B) relationships for free-rotating and fixed footings in the tests using β = 10°. It can be seen that the responses of q *vs.* S_v/B are periodic, which is due to the regular pattern of stacking of the steel rods, as mentioned earlier. The following discussion focuses on the q-S_v/B response up to the first peak value of q, which is defined as the peak value of footing pressure, q_u, as shown in Fig. 8, in which the results of all tests performed in the present study are shown. It can be seen that all curves fall within a narrow range, with different values of q_u.

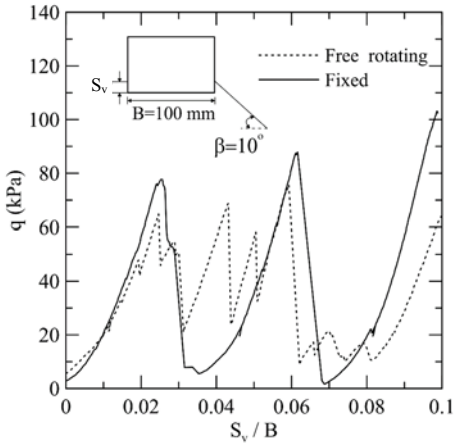

Fig. 7 Typical load-displacement curves for the tests using β = 10°

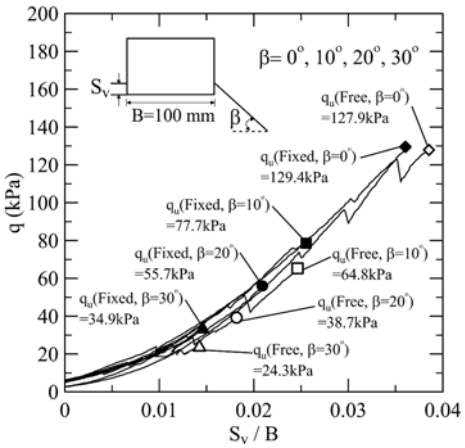

Fig. 8 Average footing pressure *vs.* footing displacement curves prior to the first peak footing load obtained in the load tests

5. OBSERVED FAILURE MECHANISM

Figures 9(a) and 9(b) show failure surfaces observed at large footing settlements (S_v = 30 ~ 50 mm) for free-rotating and fixed footings, respectively, placed on horizontal grounds (β = 0°). An active zone beneath the footing associated intensively sheared transitional and passive zones can be seen. Depths of failure mechanism are 1.1 B and 1.25 B for free-rotating and fixed footings, respectively, which are slightly affected by the rotation of footings as shown in Fig. 9(a). Figures 10, 11, and 12 compare failure mechanisms for free-rotating (Figs. 10(a), 11(a), and 12(a)) and fixed footings (Figs. 10(b), 11(b), and 12(b)), respectively, placed on slopes with β = 10°, 20° and 30°, respectively. Based on the observations in Figs. 9(a) ~ 12(b), it is clear that the failure surfaces for fixed footings develop in an area wider and deeper than those for free-rotating ones, with a minor exception in the case of β = 30°. This exception may be due to the seriously tilted footing (as shown in Fig. 12(a)) which applied a backward (or left-ward in Fig. 12(a)) load to the foundation slope. The investigation into the failure mechanisms generally suggests that deeper and wider failure zones are associated with the footing loaded with a restraint against rotations. This is true for the footing placed on horizontal ground (β = 0°) as well as on slopes (β > 0°).

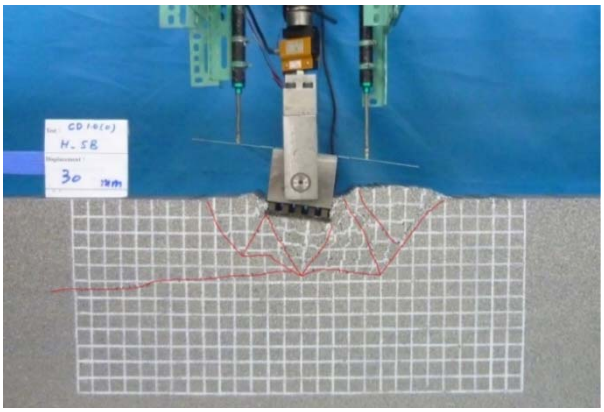

(a) At free-rotating footing

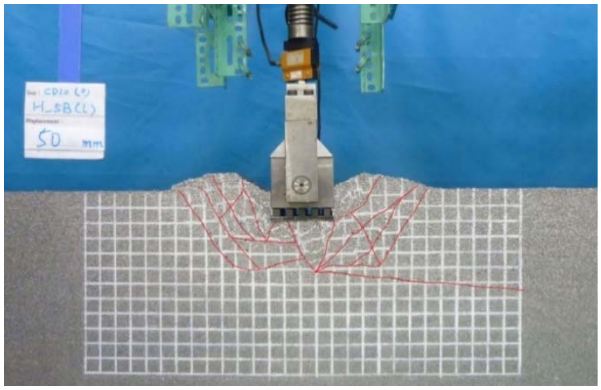

(b) At fixed footing

Fig. 9 Typical example of failure mechanisms for sloped ground (β = 0°)

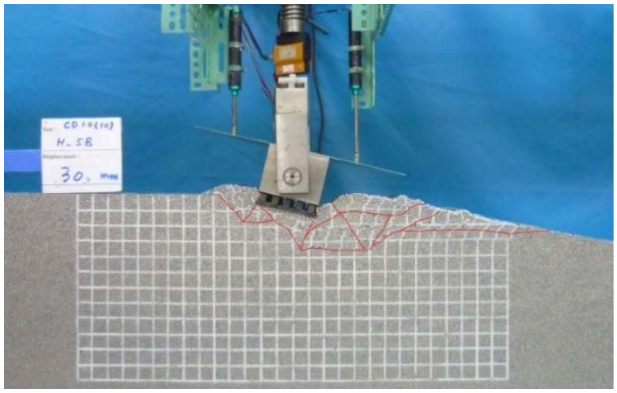

(a) At free-rotating footing

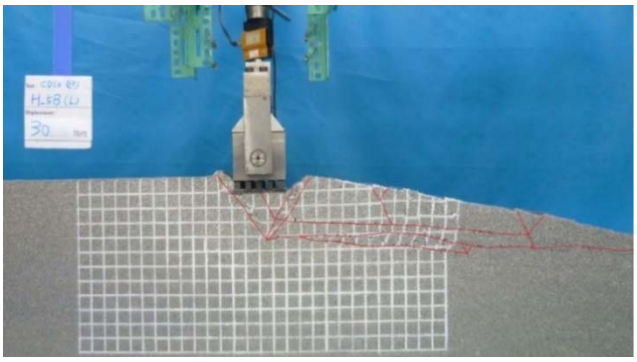

(b) At fixed footing

Fig. 10 Typical example of failure mechanisms for sloped ground (β = 10°)

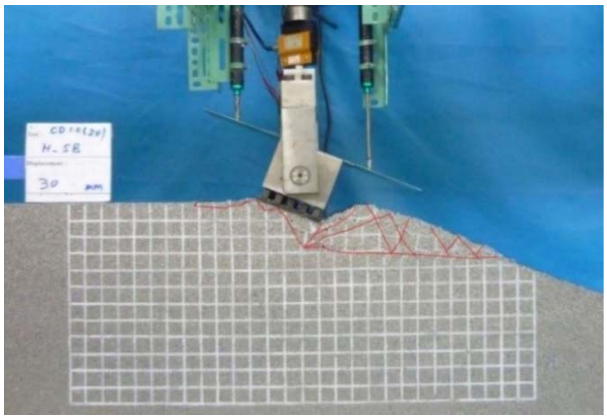

(a) At free-rotating footing

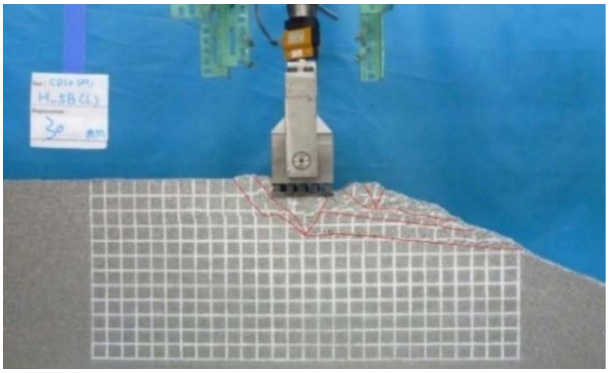

(b) At fixed footing

Fig. 11 Typical example of failure mechanisms for sloped ground (β = 20°)

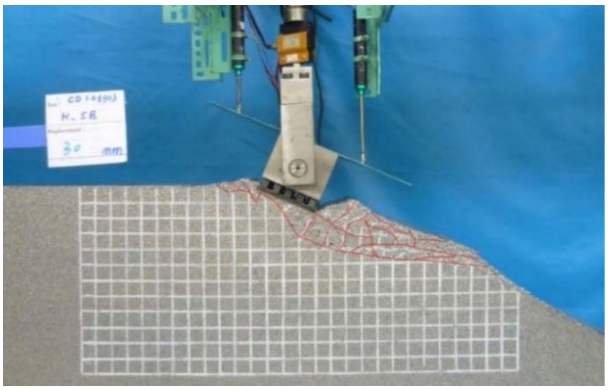

(a) At free-rotating footing

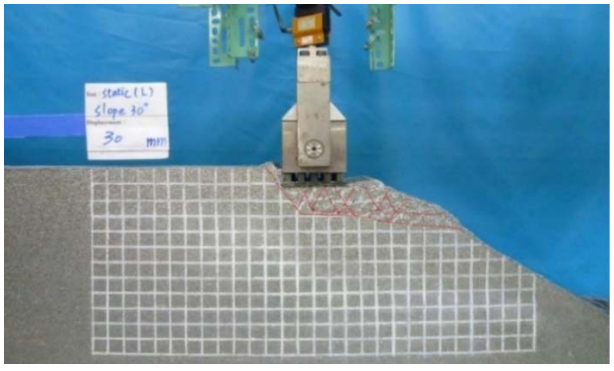

(b) At fixed footing

Fig. 12 Typical example of failure mechanisms for sloped ground (β = 30°)

6. MEASURED CONTACT PRESSURES AT FOOTING BASE

Figure 13(a) shows the distributions of normal contact pressure (q_n) at various distances (x) from the center of the footing base measured at the moment of peak loading on the free-rotating footing. The locations of the resultant normal forces at the base of the footing are also plotted. Although the curves appear slightly asymmetrical, the location of the resultant reactional force is always close to the center line of the footing. This provides the case of centric loading condition and enables a straightforward theoretical analysis using $e_c = 0$. The results of contact pressure measurements for the fixed footing are shown in Fig. 13(b). In this case, the eccentricities of the resultant reactional force tend to increase with increasing β. Figure 13(c) shows the distribution of shear stress (q_s) along the footing base measured at the moment of peak footing load for the free-rotating footing. In the case of a free-rotating footing, there are shear forces acting toward the toe of the footing at the front side and the direction of shear forces is reversed at the inner side of the footing. Figure 13(d) shows similar measurements to those shown in Fig. 13(c), except for a fixed footing. Similar patterns of shear stress distributions can be seen in these figures, regardless of the restraint condition (free or fixed) and the value of β. The results shown in Figs. 13(c) and 13(d) indicate that the influence of footing restraint (free or fixed) and slope angles (β) on the pattern of shear stress distribution is insignificant.

7. INFLUENCE OF LOAD INCLINATION AT FOOTING BASE

The load inclination angle (α) is calculated based on the normal stress ($q_{ni}, i = 1 \sim 5$) and shear stress (q_{si}) measured at the footing base using the following equation:

$$\alpha = \tan^{-1}\left(\frac{\sum q_{si}}{\sum q_{ni}}\right) \tag{3}$$

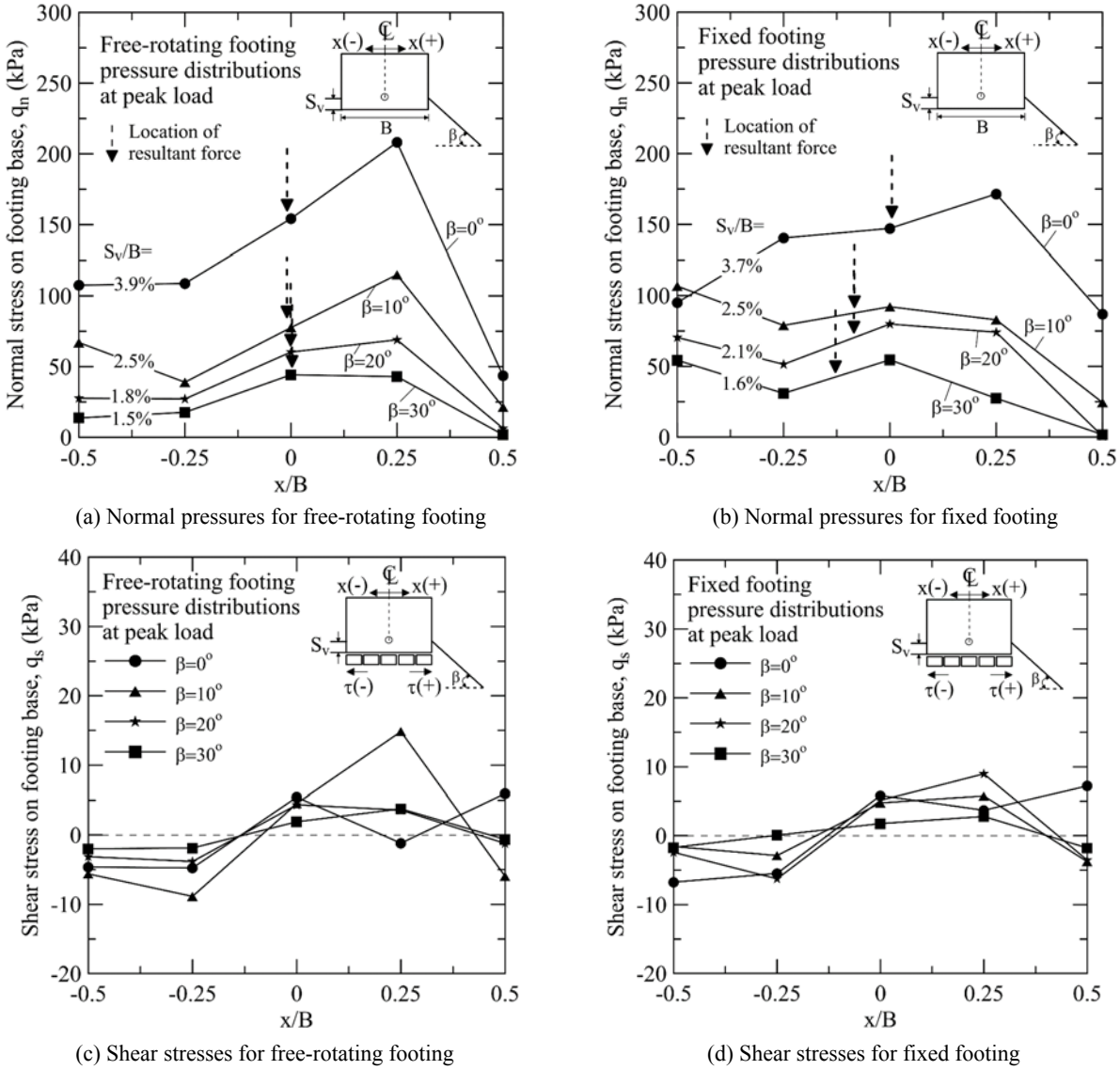

(a) Normal pressures for free-rotating footing

(b) Normal pressures for fixed footing

(c) Shear stresses for free-rotating footing

(d) Shear stresses for fixed footing

Fig. 13 Measured contact pressure distributions at footing base

The test results shown in Figs. 14(a) ~ 14(d) generally reveal that variations of the load inclination at the base of a footing subjected to a vertical load are more significant for a slanted ground (β = 30°) than those for a flat ground (β = 0°), regardless of the restraint condition on the footing (free-rotating or fixed). Figs. 14(a) ~ 14(d) also show that values of α fall within a small range of – 0.64° and +1.0° for all slope with various angles and footing restraining conditions.The following equations proposed by Meyerhof (1963) and Huang and Kang (2008), respectively, are used to evaluate possible influence of load inclination on the bearing capacity of footings:

$$i_\gamma = \left(1-\frac{\alpha}{\phi}\right)^2 \tag{4}$$

$$i_\gamma = \left(1-\frac{\alpha}{\phi}\right)^{0.1\phi-1.21} \tag{5}$$

According to Eqs. (4) and (5), i_γ ranges between 0.94 and 1.06 (for α = ±1° and φ = 35°), suggesting that the possible influence of load inclination during the loading of free-rotating and fixed footings on the value of q_u was only ±6% of q_u. However, experimental results show that variations of q_u induced by different footing restraint conditions ranged between 19% and 43% for β ≥ 10°, suggesting that the major factor influencing the value of q_u obtained in the present study is not the load inclination. Consequently, another factor, namely the load eccentricity, may account for the above-mentioned variations of q_u between the fixed and free-rotating footings.

8. INFLUENCE OF LOAD ECCENTRICITY AT FOOTING BASE

The load eccentricity e_c at the footing base is calculated using the following equation:

$$e_c = \frac{B}{2} - \frac{\sum_{i=1}^{5} q_{ni} \cdot A_i \cdot l_i}{\sum_{i=1}^{5} q_{ni} \cdot A_i} \tag{6}$$

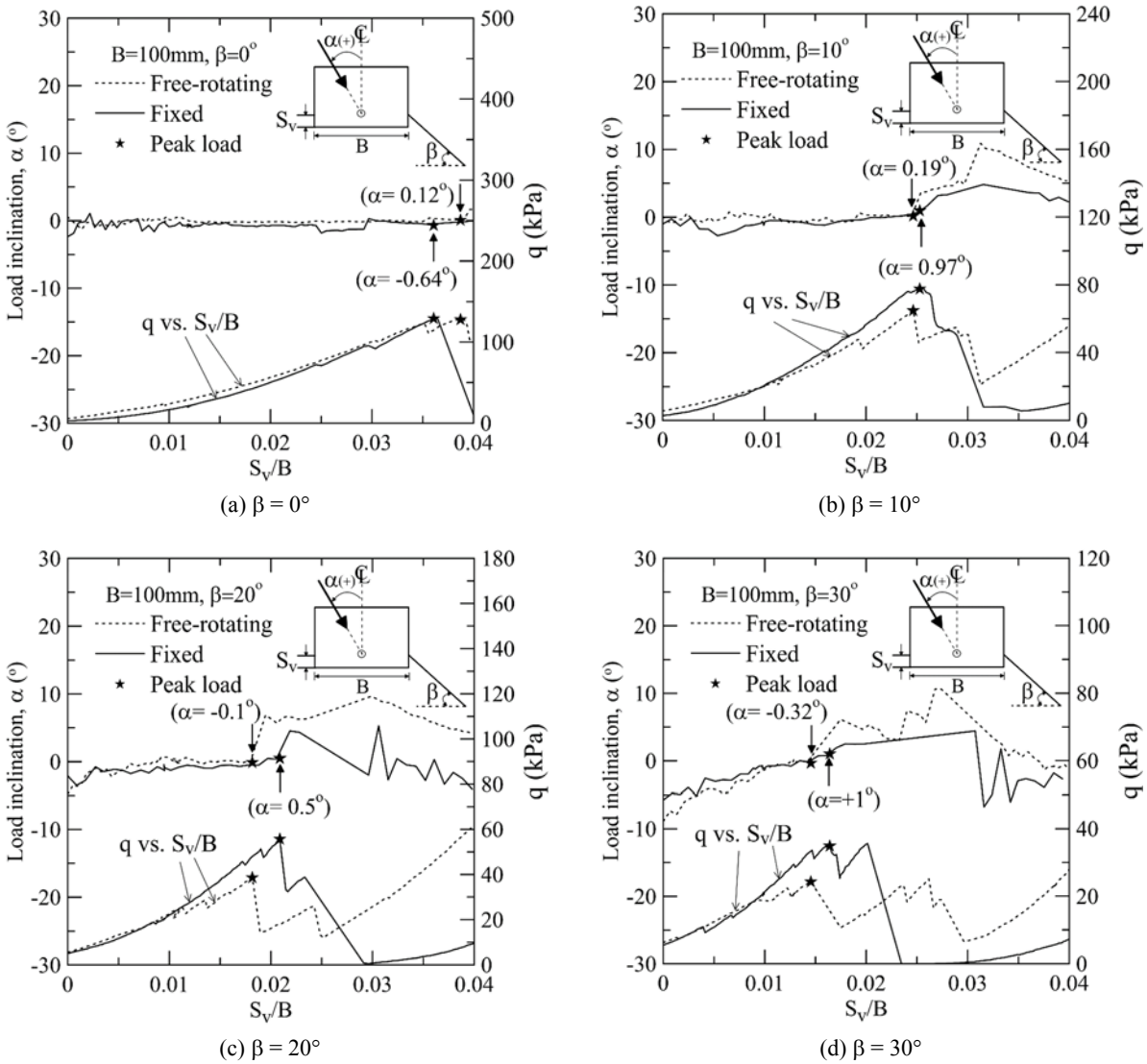

Fig. 14 Measured load inclinations at the base of footing during loading on the ground

where

q_{ni} : measured normal load for loadcell i (i = 1 – 5)

A_i : surface area of loadcell i

l_i : arm for the heel of footing to the center of loadcell i.

Figures 15(a) through 15(d) compare the measured values of load eccentrciity (e_c) between the free-rotating and fixed footings for grounds with β = 0° ~ 30°. These figures show that values of e_c for the free-rotating footing are negligibly small because the two hinges were installed as close to the footing base as possible in the present study. Figure 15(a) shows the measured load eccentricity to footing-width ratio (e_c/B) for the case of β = 0°. For the free-rotating footing, values of e_c/B = 0 throughout the process of loading (as expected). It is also seen that e_c/B = 5% at the beginning of the test is measured for the fixed footing suggesting that some mechanical issues, such as the imperfection of footing and loading frame are not negligible. Consequently, the value of e_c/B = ±5% is considered as a systematic error resulted from the imperfect footing base contact the loading system. Values of e_c/B at the beginning of the test increase with increasing β (as shown in Figs. 15(a) ~ 15(d)) are attributed to the increased influences from the asymmetric ground geometry at the two sides of footing. In the case of a fixed footing placed on the slope with β = 30°, the value of e_c/B can be as high as − 12.8%, as shown in Fig. 15(d). Comparing Figs. 15(a) ~ 15(d), a greater variation of e_c for the fixed footing than that for the free-rotating one during the loading process can be seen. Figure 15(d) also shows that the values of e_c/B decreased from about +8% (+: eccentricity toward the toe) at the beginning of loading to −12.8% (−: eccentricity toward the heel) at the moment of peak footing load. This backward load eccentricity may contribute to the increase of bearing capacity, which is not properly addressed in existing theories and equations. A commonly used approach for determining the effect of load eccentricity on the footing is the use of the effective base width proposed by Meyerhof (1953), expressed as:

$$B' = B - 2 \cdot e_c \tag{7}$$

Based on the above-mentioned theory of effective footing width, the correction factor e_γ can be defined as:

$$e_\gamma = \frac{B'}{B} \tag{8}$$

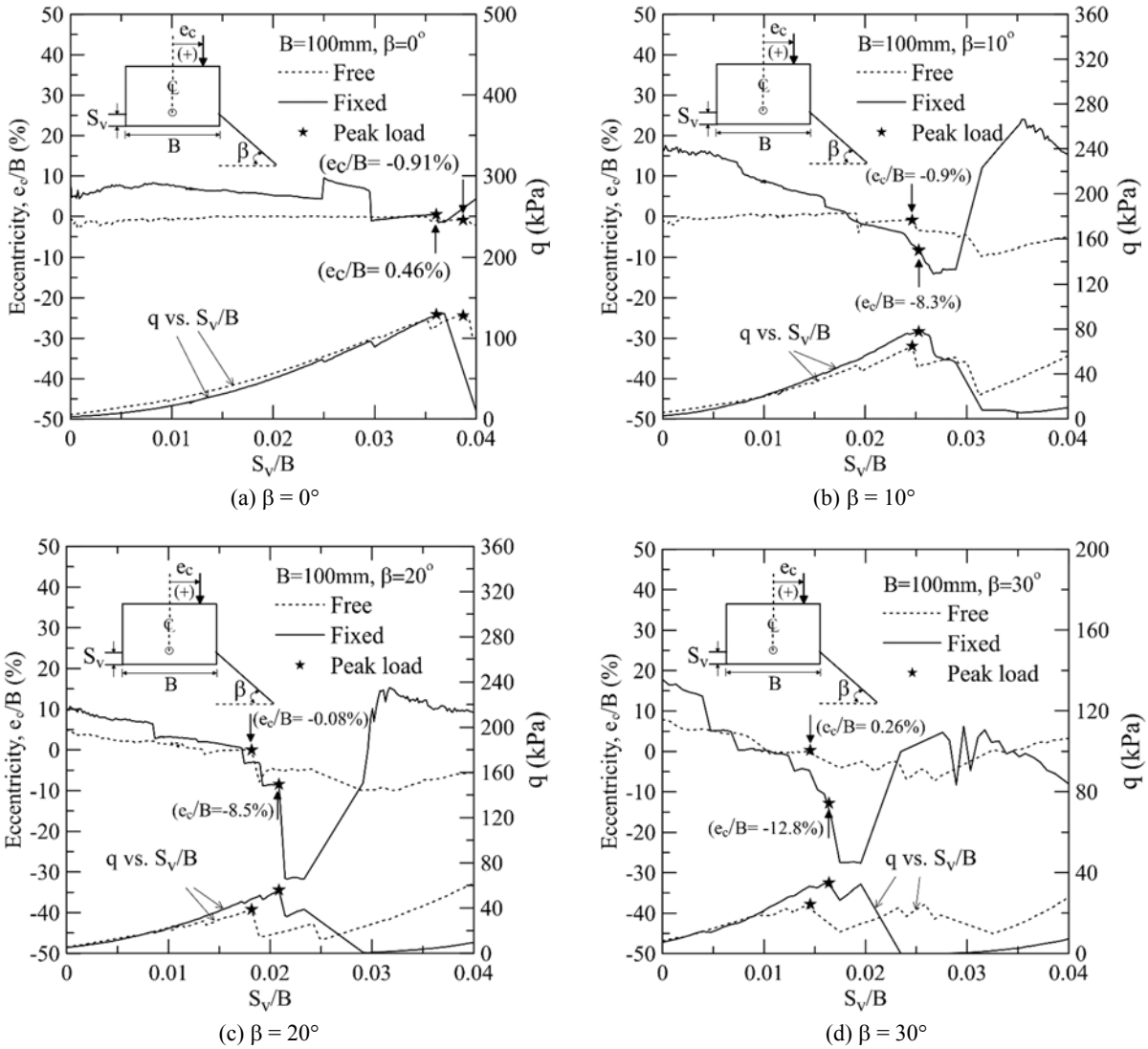

Fig. 15 Measured load eccentricity at the base of footing during loading on the ground

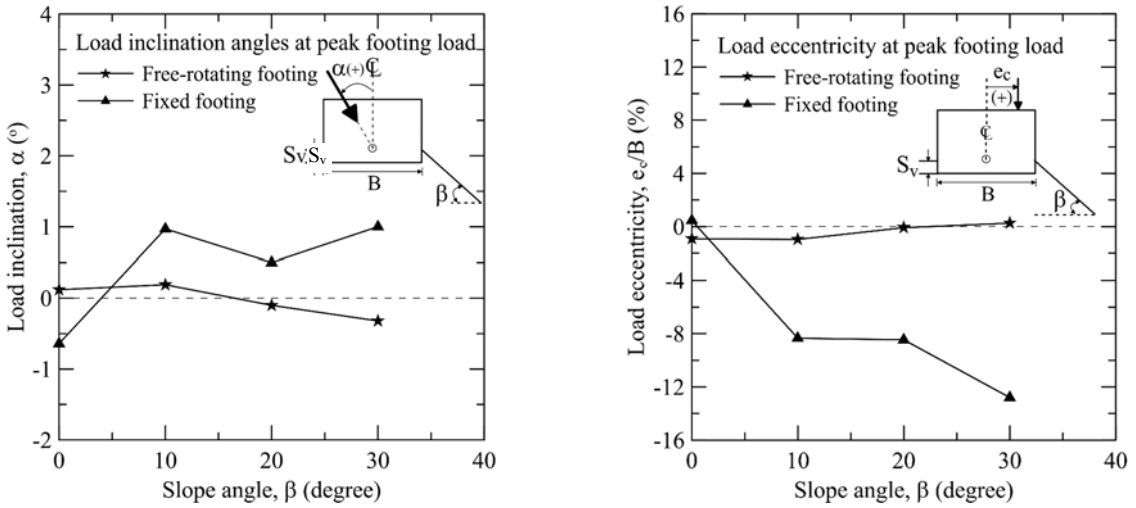

(a) Load inclination angles *vs.* slope angle at peak footing load (b) Load eccentricity *vs.* slope angle at peak footing load

Fig. 16 Experimental values of load inclination angles and load eccentricity

Figure 16(a) shows measured values of α *vs.* β for free-rotating and fixed footings at the moment of peak footing load. Although an increasing trend of α versus increasing β can be seen for the free-rotating footing, variations of α for the fixed and free-rotating footings are generally as small as $-1° < \alpha < +1°$, and thus α is not a major factor influencing the ultimate bearing capacity of footings, as discussed earlier. Figure 16(b) shows the value of e_c/B *vs.* β measured at the moment of peak footing load. A clear trend of increasing e_c/B (toward the heel side of the footing) versus β in the case of a fixed footing can be seen. On the other hand, values of e_c/B are nearly zero regardless of the value of β for the free-rotating footing. A detailed analytical investigation on the effect of this backward load eccentricity (negative value of e_c/B) on the ultimate bearing capacity will be reported in a follow-up study.

10. CONCLUSIONS

A series of loading tests on model horizontal grounds and slopes consisting of idealized two-dimensional round particles was performed using a strip footing with different constraint conditions, namely free-rotating and fixed footings. Five load cells that can detect normal and shear forces simultaneously with a negligibly small coupling effect were used to measure the contact pressures of the footing base, allowing straightforward and detailed investigations of the influence of load inclination and load eccentricity on the behavior of footings placed on horizontal and slanted grounds. Test results reveal that by imposing a rigid restraint against the rotation of the footing, a larger value of ultimate bearing capacity, associated with a failure surface deeper than that for the footing with no rotation constraint, can be obtained. This is true for all slope angles in the range of 0° to 30° investigated in the present study. However, the full restraint condition (*i.e.,* fixed footing) used here requires a strong external support from the superstructure in practice. Model test results reveal that the relatively deep failure mechanism and relatively large values of ultimate bearing capacity (q_u) for the rigidly restrained (fixed) footing are the result of a relatively large load eccentricity (e_c) toward the heel side of the footing base. This observation contradicts the common knowledge that a load eccentricity at the footing base reduces the value of q_u, suggesting that the common practice on the bearing capacity evaluation for footings placed on a horizontal ground may not be applicable for the case of near-slope footings.

ACKNOWLEDGEMENTS

This study was financially supported by the Ministry of Science and Technology, Taiwan, under research grant MOST 107-2221-E-006-043-MY2.

REFERENCES

ASTM International (2017). *ASTM D-2487 Standard Practice for Classification of Soils for Engineering Pusposed (Unified Soil Classification System)*. West Conshohocken, PA, USA.

Briaud, J.L. and Gibben, R. (1999). "Behaviour of five large scale spread footings in sand." *Journal of Geotechnical and Geoenvironmental Engineering*, ASCE, **125**(9), 787-796. https://doi.org/10.1061/(ASCE)1090-0241(1999)125:9(787)

Cure, E., Sadoglu, E., Turker, E., and Uzuner, B.A. (2014). "Decrease trends of ultimate loads of eccentrically loaded model strip footings close to a slope." *Geomechanics and Engineering*, **6**(5), 469-485. https://doi.org/10.12989/gae.2014.6.5.469

Duncan, J.M. and Wright, S.G. (2005). *Soil Strength and Slope Stability*. John Willey & Sons.

El-Sawwaf, M. (2009) "Experimental and numerical study of eccentrically loaded strip footings resting on reinforced sand." *Journal of Geotechnical and Geoenvironmental Engineering*, ASCE, **135**(10), 1509-1518. https://doi.org/10.1061/(ASCE)GT.1943-5606.0000093

El Sawwaf, M. and Nazir, A. (2012). "Behavior of eccentrically loaded small-scale ring footings resting on reinforced layered soil." *Journal of Geotechnical and Geoenvironmental Engineering*, ASCE, **138**(3), 376-384. https://doi.org/10.1016/j.jare.2011.10.002

Fishman, K.L., Richards, R.J., and Yao, D. (2003). "Inclination factors for seismic bearing capacity." *Journal of Geotechnical and Geoenvironmental Engineering*, ASCE, **219**(9), 861-865. https://doi.org/10.1061/(ASCE)1090-0241(2003)129:9(861)

Ganesh, R., Khuntia, S., and Sahoo, J.P. (2017). "Bearing capacity of shallow strip foundation under eccentric and oblique loads." *In-*

ternational Journal of Geomechanics, ASCE, **17**(4), 06016028(1-8). https://doi.org/10.1061/(ASCE)GM.1943-5622.0000799

Georgiadis, K. (2010). "An upper-bound solution for the undrained bearing capacity of strip footings at the top of a slope." *Geotechnique*, ASCE, **60**(10), 1-6. https://doi.org/10.1061/(ASCE)GT.1943-5606.0000373

Hansen, J.B. (1970). *A Revised and Extended Formula for Bearing Capacity*. Danish Geotechnical Institute, Copenhagen, Bulletin No. 28.

Huang, C.-C. and Chen, Y.-S. (2012a). "Behaviour of reinforced structures under simulated toe scouring." *Geosynthetics International*, **19**(4), 272-283. https://doi.org/10.1680/gein.12.00014

Huang, C.-C. and Chen, Y.-S. (2012b). "Stability analysis of reinforced walls subjected to simulated toe scouring" *Geosynthetics International*, **19**(4), 284- 291. http://dx.doi.org/10.1680/gein.12.00015

Huang, C.-C. and Kang, W.-W. (2008). "The effect of a setback on the bearing capacity of a surface footing near a slope." *Journal of GeoEngineering*, TGS, **3**(1), 25-32. https://doi.org/10.6310/jog.2008.3(1).3

Huang, C.-C, Tatsuoka, F. and Sato, Y. (1994). "Failure mechanisms of reinforced sand sloped loaded with a footing." *Soils and Foundations*, **34**(2), 27-40. https://doi.org/10.3208/sandf1972.34.2_27

Krabenhoft, S., Damkilde, L. and Krabbenhoft, K. (2013). "Bearing capacity of strip footings in cohesionless soil subjected to eccentric and inclined loads." *Internal Journal of Geomechanics*, ASCE, **14**(3), 04014003(1-18). https://doi.org/10.1061/(ASCE)GM.1943-5622.0000332

Kumar, J. and Chakraborty, M. (2015). "Bearing capacity factors for ring foundations." *Journal of Geotechnical and Geoenvironmental Engineering*, ASCE, **141**(10), 06015007(1-7). https://doi.org/10.1061/(ASCE)GT.1943-5606.0001345

Leshchinsky, B. (2015). "Bearing capacity of footings placed adjacent to c′-ϕ′ slopes." *Journal of Geotechnical and Geoenvironmental Engineering*, ASCE, **141**(6), 04015022(1-13). https://doi.org/10.1061/(ASCE)GT.1943-5606.0001306

Leshchinsky, B. and Xie, Y. (2017). "Bearing capacity for spread footings placed near c′-φ′ slopes." *Journal of Geotechnical and Geoenvironmental Engineering*, ASCE, **143**(1), 06016020(1-5). https://doi.org/10.1061/(ASCE)GT.1943-5606.0001578

Meyerhof, G.G. (1953). "The bearing capacity of foundations under eccentric and inclined loads." *Proceeding of 3rd International Conference on Soil Mechanics and Foundation Engineering*, **1**, 440-445.

Meyerhof, G.G. (1957). "The ultimate bearing capacity of foundations on slopes." *Proceedings of 4th ICSMFE,* London, **1**, 384-386.

Meyerhof, G. G. (1963). "Some recent research on the bearing capacity of foundations." *Canadian Geotechnical Journal*, **1**(1), 16-26. https://doi.org/10.1139/t63-003

Purkayastha, R.D. and Char, R.A.N. (1977). "Stability analysis of eccentrically loaded footings." *Journal of Geotechnical Engineering Division*, ASCE, **103**(6), 647-651.

Sadoglu, E. (2015). "Numerical analysis of centrally and eccentrically loaded strip footing on geotextile-reinforced sand." *Geosynthetics International*, **22**(3), 225-234. https://doi.org/10.1680/gein.15.00007

Kotake, N., Tatsuoka, F., Tanaka, T., Siddiquee, M.S.A., and Huang, C.-C. (2001). "FEM simulation of the bearing capacity of level reinforced sand ground subjected to footing load." *Geosynthetics International*, **8**(6), 501-549. https://doi.org/10.1680/gein.8.0205

Tang, Y., Taiebat, H.A., and Senetakis, K. (2017). "Effective stress based bearing capacity equations for shallow foundations on unsaturated soils." *Journal of GeoEngineering*, TGS, **12**(2), 59-64. http://dx.doi.org/10.6310/jog.2017.12(2).2

Tatsuoka, F. and Huang, C.-C. (1991). Discussion on "Bearing capacity of foundations in slopes." *Journal of Geotechnical Engineering*, ASCE, **117**(12), 1970-1975. https://doi.org/10.1061/(ASCE)0733-9410(1991)117:12(1970.2)

Terzaghi, K. (1943). *Theoretical Soil Mechanics*, New York, Wiley. https://doi.org/10.1002/9780470172766

Ukritchon, B., Whittle, A.J. and Klangvijit, C. (2003). "Calculations of bearing capacity factor N_γ using numerical limit analyses." *Journal of Geotechnical and Geoenvironmental Engineering*, ASCE, **129**(5), 468-474. https://doi.org/10.1061/(ASCE)1090-0241(2003)129:6(468)

Vesic, A.S. (1973). "Analysis of ultimate loads of shallow foundations." *Journal of Soil Mechanics and Foundation Division*, ASCE, **99**(1), 45-73.

Vesic, A.S. (1975). *Foundation Engineering Handbook*, Chap. 3, 1st Ed., Winterkorn, H. F. and Fang, H. Y., Eds., Van Nostrand Reinfold, New York, 751pp.

Zhu, M. and Michalowski, R.L. (2005). "Shape factors for limit loads on square and rectangular footings." *Journal of Geotechnical and Geoenvironmental Engineering*, ASCE, **131**(2), 223-231. https://doi.org/10.1061/(ASCE)1090-0241(2005)131:2(223)